Catalysis Science & Technology

Accepted Manuscript

ROYAL SOCIETY OF CHEMISTRY

www.rsc.org/catalysis

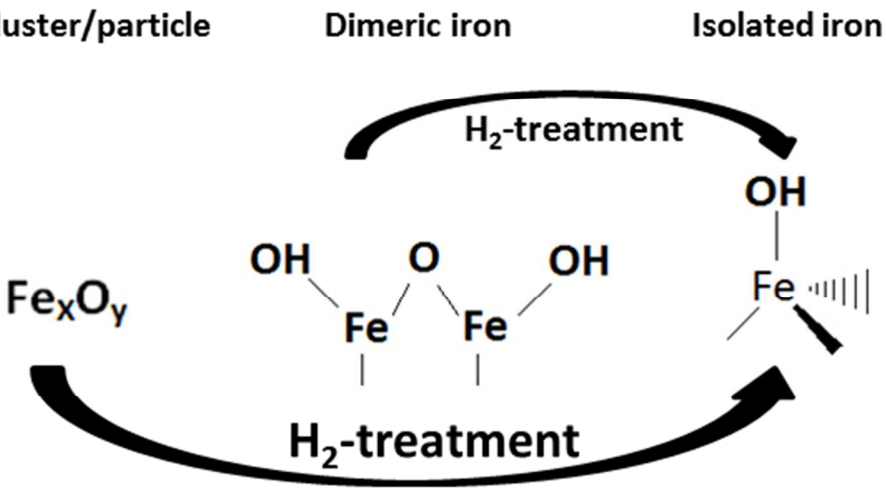

159x78mm (96 x 96 DPI)

Effect of post-synthesis hydrogen-treatment on the nature of iron species in Fe-BEA as NH_3-SCR catalyst

Soran Shwan[a,*], Jonas Jansson[b], Louise Olsson[a] and Magnus Skoglundh[a]

[a] Competence Centre for Catalysis, Chalmers University of Technology, SE-412 96 Gothenburg, Sweden

[b] Volvo Group Trucks Technology, SE-40508, Gothenburg, Sweden

[*] Corresponding author:
Soran Shwan
Competence Centre for Catalysis and
Department of Applied Surface Chemistry
Chalmers University of Technology
SE-41296 Göteborg, Sweden

Telephone: +46 (0)31 772 2943
Email: soran@chalmers.se

Abstract

Post-synthesis treatment of Fe-BEA with hydrogen has previously been shown to improve the low-temperature activity for NO reduction during standard NH_3-SCR. Here, a 2 wt. % Fe-BEA sample was prepared by incipient wetness impregnation and calcined in air at 450°C for 3 h. The fresh sample was then treated with 5 % H_2 at 650^0C for 5 h. The evolution of different iron species in Fe-BEA before and after H_2-treatment was studied using *in situ* DRIFT spectroscopy with NO as probe molecue, and by UV-Vis spectroscopy. The DRIFTS results show that the relative intensity of the absorption peak representing isolated iron species increases significantly after H_2-treatment of the fresh Fe-BEA sample. Furthermore, the UV-Vis results show a significant decrease in the relative intensity in the UV region representing larger iron particles wheareas the relative intensity representing smaller iron species increases after treatment of Fe-BEA with hydrogen. The results show that the low-temperature NO reduction during standard NH_3-SCR can be increased for Fe-BEA by redispersion of smaller iron species into the zeolite structure by hydrogen-treatment.

Keywords: Selective catalytic reduction; NH_3-SCR; Low-temperature activity; Zeolite beta; BEA; Fe-BEA; Iron; Iron species; Post-synthesis treatment; Hydrogen-treatment; NO adsorption, *in situ* DRIFT spectroscopy, UV-Vis Spectroscopy

1. Introduction

Iron- [1-6] and copper- [3, 7-11] exchanged zeolites are presently the most common and promising NO_X reduction catalysts for mobile NH_3-SCR applications. In general, copper-exchanged zeolites have higher low-temperature activity whereas iron-exchanged zeolites have higher high-temperature activity for SCR. According to several studies, monomeric Fe^{3+} [12-23] and binuclear $[HO\text{-}Fe\text{-}O\text{-}Fe\text{-}OH]^{2+}$ [12-15, 21-27] iron species are suggested to be the active species for low- and high-temperature SCR, respectively. Furthermore, larger iron oxides particles [14, 15, 28] are suggested to be the governing iron species for NO oxidation.

To achieve an improved low-temperature SCR activity for iron-exchanged zeolites, different methods may be applied [1]. Iwasaki et al. [29] showed that the SCR activity for Fe-ZSM-5 can be improved by hydrogen-treatment of the sample. In a recent study by our group [30], the low-temperature SCR activity for iron-exchanged zeolite BEA (Fe-BEA) was significantly improved by post-synthesis treatment of the sample using hydrogen. The increased activity was suggested to be due to breaking of iron oxide clusters into smaller iron species, which probably are stabilized by forming stronger bonds to the zeolite matrix. However, the exact nature of the improved low-temperature activity due to hydrogen-treatment of Fe-zeolites is still unclear and not determined. Furthermore, in another recent study [21], the dynamics of the active iron species before and after thermal treatment was studied using *in situ* FTIR spectroscopy with NO as probe molecule and correlated to a broad range of activity measurements and characterization techniques. A variety of iron species, active for NO adsorption, were identified and the evolution of these species was followed after thermal treatment. The results showed that smaller iron species (monomeric and dimeric) form oligomeric iron clusters after short time of ageing whereas longer time of thermal treatment results in formation of larger iron oxide particles.

The aim of the present study is to give an increased understanding of the mechanism improving the low-temperature activity after post-synthesis treatment with hydrogen. The evolution of the different iron species of Fe-BEA are studied after hydrogen-treatment by hydrogen using *in situ* FTIR spectroscopy with NO as probe molecule as well as X-ray diffraction and diffuse-reflectance UV-Vis

spectroscopy. The results in the present study are correlated with activity data from our recent study of hydrogen-treated Fe-BEA [30].

2. Experimental Methods

2.1. Material

A 2 wt. % Fe-BEA catalyst prepared by incipient wetness impregnation is used in the present study. 9.8 g H-BEA (SAR=38, Zeolyst International) powder was dried at 120^{0}C for 2 h and 1.44 g $Fe(NO_3)_3 \cdot 9H_2O$ (Fisher Scientific) was dissolved in 9.8 ml distilled water. The iron nitrate solution was carefully mixed with the dried H-BEA powder and then dried again at 120^{0}C for 24 h before crushed into a fine powder and finally calcined in air at 450^{0}C for 3 h.

2.2. Post-synthesis treatment with hydrogen

The 2 wt. % Fe-BEA powder catalyst was treated with hydrogen using a continuous gas flow reactor system which is described in more detail in ref. [7]. A cordierite monolith substrate (Corning; 400 cpsi; 21 mm in diameter and 60 mm in length) was prepared where the inner parts were cut out in an oval shape. The Fe-BEA powder was spread inside the monolith before placed inside the quartz tube. The gas flow through the reactor during the hydrogen-treatment was 3500 ml/min and consisted of 5 % H_2 and Ar as inert gas and the temperature was kept at 650°C for 5 h. Before the high-temperature H_2-treatment the sample was exposed to the same gas composition at 30^{0}C in order to eliminate any species which can act as oxidants at high temperatures and thereafter the temperature was increased using the same gas mixture (5 % H_2 in Ar). Furthermore, after the hydrogen-exposure, the sample was first flushed with Ar for 10 min at 650^{0}C and then exposed to 8 % O_2 for another 5 h before cooled to room temperature.

2.3. X-ray diffraction

X-ray diffraction (XRD) was used to identify any changes of crystalline phases of the sample due to the hydrogen-treatment. The XRD instrument used was a Siemens D500 X-ray diffractometer with Bragg-Brentano geometry and a Cu Kα source. The main BEA zeolite diffraction peaks at 2θ = 7.74

and 22.7^0 [31, 32] were studied before and after hydrogen-treatment. Furthermore, the region with diffraction peaks characteristic for iron oxide, Fe_2O_3, at $2\theta = 33.2$ and 35.5^0 [33] was also examined.

2.4. FTIR spectroscopy

In situ FTIR spectroscopy was used to follow the evolution of surface species on the samples. Spectra were recorded with a BioRad FTS 6000 spectrometer in diffuse reflectance mode where the sample (about 50 mg) was placed in an *in situ* flow reactor (Harrick Praying Mantis DRIFT cell). The total gas flow was kept constant at 400 mL/min using argon as balance and separate mass flow controllers (Bronkhorst Hi-Tech) for NO, O_2 and Ar were used to control the feed gas composition. The IR spectra were recorded with a spectral resolution of 1 cm^{-1} where background spectra were taken in Ar with the same spectral resolution prior to each experiment at the same temperature as the subsequent experiment. Before the experiments the samples were pretreated in a flow of Ar and 5 % O_2 at 500^0C for 1 hour. Adsorption experiments using NO as probe molecule were performed for both fresh H-BEA and Fe-BEA samples, and for the H_2-treated Fe-BEA sample by exposing the sample to 400 ppm NO for 30 min at 150^0C, where DRIFT spectra continuously were recorded during the adsorption process until saturation.

2.5. UV-Vis spectroscopy

The fresh H-BEA, Fe-BEA, and hydrogen-treated Fe-BEA samples were further characterized using diffuse reflectance UV-Vis spectroscopy to detect any changes of the iron species. UV-Vis Spectra were recorded in the 200-1500 nm wavelength range using a Cary 5000 UV-Vis-NIR spectrophotometer equipped with an external DRA-2500 unit. The UV-Vis spectrum of H-BEA was thereafter subtracted from the corresponding spectrum for Fe-BEA spectrum in order to achieve the spectrum for iron before and after hydrogen-treatment. The UV-Vis spectra for iron were converted using the Kubelka-Munk function and deconvoluted using a Gaussian function. The UV-Vis equipment is described in more detail in ref. [22].

3. Results and discussion

3.1. Characterization

Figure 1 shows the X-ray diffractograms for fresh and hydrogen-treated Fe-BEA, and the corresponding diffractogram for the fresh H-BEA sample. For the Fe-BEA samples, there are no significant diffraction peaks at $2\theta = 33.2$ or 35.5^0 [33] representing Fe_2O_3. This indicates that Fe_2O_3 particles are either too small to be identified with XRD or that iron oxide is present as non-crystalline phases in the Fe-BEA samples. Furthermore, the characteristic diffraction peaks for zeolite BEA at $2\theta = 7.74$ and 22.7^0 [31, 32] can be observed for all samples. Our recent study of 2 wt. % Fe-BEA showed a significant decrease in zeolite acidity after hydrogen-treatment [30] where the NH_3 storage capacity decreased from 0.656 to 0.555 mmol/g. Furthermore, a clear correlation between zeolite crystal size and NH_3 storage capacity of the zeolite has previously been observed [14]. It was shown that a decrease in NH_3 storage capacity due to hydrothermal treatment could be correlated with a decrease in mean crystal size of the zeolite indicating dealumination. However, there are no clear differences between the X-ray diffractograms in Figure 1 indicating that the structure of Fe-BEA is not affected by the hydrogen-treatment. In another study we have shown that the ammonia storage capacity decreases when introducing iron into the zeolite [23]. It was suggested that the iron species exchanged into the zeolite decreases the number of Brønsted sites available for ammonia storage. Hence the decreased acidity of the samples after hydrogen-treatment is most likely due to loss of available acid sites due to re-dispersion of iron (cf. 3.2).

To study the changes in distribution of iron species after hydrogen-treatment of the Fe-BEA sample, diffuse reflectance UV-Vis spectroscopy was used. Figure 2 shows the UV-Vis spectra for iron for the fresh and H_2-treated Fe-BEA samples. The deconvoluted spectra show two bands in the lower wavelength region with maxima at 234 and 274 nm. These bands are related to isolated Fe^{3+} species [34, 35]. The bands with maxima at 328 and 389 nm are assigned to dimeric iron (Fe^{2+}) species and smaller oligomeric Fe species as Fe_xO_y inside the zeolite pores [34, 35]. Finally, the band with maximum at 466 nm is related to Fe_2O_3 particles located outside the zeolite pores [34, 35]. The relative intensities of the deconvoluted peaks are summarized in Table 2. After hydrogen-treatment,

there is a clear decrease in peak intensity for the peaks III-V, representing larger iron species, while the intensity of the peaks related to isolated iron species, peaks I-II, increases. This is in accordance with the results from our previous activity study [30] for the same catalyst, where the NO conversion during standard NH_3-SCR (400 ppm NO and NH3, 8% O_2 and 5% H_2O) increases significantly after hydrogen-treatment. Table 2 summarizes the NO conversion over fresh and H_2-treated Fe-BEA during standard NH_3-SCR conditions between 150 and 500^{0}C. In Table 2 it can be observed that the NO reduction at low temperatures (<300^{0}C) increases significantly after hydrogen-treatment of the sample. Furthermore, Table 2 also shows that the NO conversion at high temperatures (>400^{0}C) decreases after hydrogen-treatment. This is also in line with our previous studies [14, 15, 21-23, 30, 36], where it is suggested that dimeric iron species are active for high-temperature SCR. The results in Figure 2 and Table 2 show that the assigned dimeric iron species represented by the third and fourth deconvoluted peaks, slightly decrease, which can be correlated with the decreased high-temperature SCR activity after hydrogen-treatment of the Fe-BEA sample.

3.2. NO adsorption

Figure 3 shows the results from the *in situ* DRIFT study for fresh H-BEA and Fe-BEA compared to H_2-treated Fe-BEA. The spectra shown were recorded just after the samples were saturated with nitric oxide during NO exposure at 150^{0}C. Three distinct absorption peaks centered around 2134, 1880-1870 and 1635 cm^{-1} can be seen in the spectra. The assignment of the peaks are summarized in Table 1. The H-BEA sample shows an absorption peak at 2134 cm^{-1} which is assigned to stretching vibrations of ionic NO^+ species bound to Brønsted acid sites in the zeolite [37-39]. Furthermore, this peak is slightly more intense for the Fe-BEA samples compared to the H-BEA sample. We observed similar results in our previous study of 1 wt. % Fe-BEA where the peak centered at 2134 cm^{-1} was slightly more intense for Fe-BEA than for the H-BEA sample [21]. Hence, the absorption peak at 2134 cm^{-1} may also be assigned to NO^+ ions bound to Fe^{3+} sites [40-43]. Furthermore, for the hydrogen-treated sample, the absorption peak at 2134 cm^{-1} remains relatively unchanged compared to the corresponding peak for the fresh Fe-BEA sample, indicating that the H_2-treatment does not affect the adsorption of NO^+ at the corresponding wavenumber.

Absorption bands in the range 1900-1850 cm^{-1} represent NO_X adsorbed on different iron species [38, 44-46]. The spectra show two overlapping peaks at 1880 and 1870 cm^{-1}, representing NO_X adsorbed on isolated iron species (Fe^{3+} or Fe^{2+}) [38, 44-46] and oligomeric iron clusters (Fe_xO_y) located in the porous system of zeolite BEA, respectively [38, 44]. The hydrogen-treated Fe-BEA sample shows a clear and strong relative increase in absorption of the band in the range 1900-1850 cm^{-1} compared to the fresh Fe-BEA sample. Furthermore, the relative increase in absorption peak for the hydrogen-treated sample is most likely due to an increase of isolated rather than oligomeric iron species. This is in accordance with the UV-Vis results which show a relative increase of isolated iron species and decrease in oligomeric iron species, hence the increase in absorption in the range 1900-1850 cm^{-1} is most likely due to an increase of isolated iron species. It was suggested in our recent study of hydrogen treated Fe-BEA [30], that H_2-treatment likely results in the formation of new isolated iron species increasing the low-temperature SCR activity which is in agreement with the present results. Table 2 shows a significant increase in low-temperature SCR activity after hydrogen-treatment of the Fe-BEA sample which is in line with our previous results [14, 15, 21-23, 30, 36] where it is suggested that monomeric iron species are the governing active species for the low-temperature ($<300^0C$) SCR activity over this type of catalyst.

The absorption peaks around 1635 cm^{-1} in Figure 3, represent NO_2 adsorbed on Fe-species [29, 46, 47]. The structure of the iron species giving rise to the NO_X absorption at 1635 cm^{-1} was discussed by Mul et al. who concluded that these species are larger nano-particles, Fe_2O_3, located outside the zeolite pores [38]. For the hydrogen-treated Fe-BEA sample in the present study the intensity of the absorption peak at 1635 cm^{-1} decrease slightly the UV-Vis results show a more substantial decrease of the relative amount of iron particles compared to the fresh sample. When compared, these results seem contradicting. However, the UV-Vis results do not show the number of iron sites available for NO adsorption, but the total amount of iron, while the DRIFTS results are related to adsorption of NO_2. We have previously shown [14, 15, 21] that an increased number of iron particles may lead to a decreased total surface area available for NO_X adsorption due to particle growth. The results in the present study indicate that the number of iron particle sites available for NO_2 adsorption may not be

significantly affected by the hydrogen-treatment under the present conditions. However, the total amount of iron in iron particles decreases when smaller iron species are formed.

4. Concluding remarks

The objective of the present study was to give a better understanding of the mechanism improving the low-temperature SCR activity of Fe-BEA after post-synthesis H_2-treatment. Using *in situ* DRIFT spectroscopy with NO as probe molecule, X-ray diffraction and diffuse-reflectance UV-Vis spectroscopy the dynamics of the different iron species of a 2 wt. % Fe-BEA sample are investigated. The present results are correlated to previous studies of the same catalyst by our group.

In a recent work by our group, it was found that hydrogen-treatment of Fe-BEA results in increased low-temperature (<300^{0}C) activity for NH_3-SCR, while the corresponding high-temperature (>400^{0}C) activity slightly decreased. It was suggested that the increase in activity after hydrogen-treatment may be due to formation of smaller iron species bound to the zeolite structure. The results in the present study show that the relative amount of monomeric- iron species increases after hydrogen-treatment, which previously have been suggested to be the governing iron species for low-temperature SCR. Furthermore, the hydrogen-treatment of Fe-BEA showed a decrease of the relative amount of larger iron species (dimeric and oligomeric iron species, and iron particles). This agrees well with the decreased high-temperature activity for NH_3-SCR which is suggested to be governed by dimeric-iron species.

The results in the present study are in agreement with the results from our previous studies of Fe-BEA. The different iron species present in Fe-BEA have been identified and the dynamics of these species are followed before and after post-synthesis treatment with hydrogen. We have been able to follow and show the change of the nature of the iron species due to hydrogen-treatment of Fe-BEA which results in a significant increase of low-temperature NH_3-SCR activity.

5. Acknowledgments

This work has been performed within the FFI program (Proj. No. 32900-1), which is financially supported by the Swedish Energy Agency and partly within the Competence Centre for Catalysis, which is hosted by Chalmers University of Technology and financially supported by the Swedish Energy Agency and the member companies AB Volvo, Volvo Car Corporation AB, Scania CV AB, Haldor Topsøe A/S, and ECAPS AB. Financial support from Knut and Alice Wallenberg Foundation, Dnr KAW 2005.0055, is gratefully acknowledged.

References

[1] S. Brandenberger, O. Krocher, A. Tissler, R. Althoff, Catal. Rev.-Sci. Eng. 50 (2008) 492-531.

[2] A. Grossale, I. Nova, E. Tronconi, D. Chatterjee, M. Weibel, J. Catal. 256 (2008) 312-322.

[3] K. Rahkamaa-Tolonen, T. Maunula, M. Lomma, M. Huuhtanen, R.L. Keiski, Catal. Today 100 (2005) 217-222.

[4] A. Grossale, I. Nova, E. Tronconi, Catal. Today 136 (2008) 18-27.

[5] O. Kröcher, M. Devadas, M. Elsener, A. Wokaun, N. Söger, M. Pfeifer, Y. Demel, L. Mussmann, Applied Catalysis B: Environmental 66 (2006) 208-216.

[6] A. Grossale, I. Nova, E. Tronconi, Catal. Lett. 130 (2009) 525-531.

[7] H. Sjövall, L. Olsson, E. Fridell, R.J. Blint, Applied Catalysis B: Environmental 64 (2006) 180-188.

[8] S. Kieger, G. Delahay, B. Coq, B. Neveu, J. Catal. 183 (1999) 267-280.

[9] J.H. Park, H.J. Park, J.H. Baik, I.S. Nam, C.H. Shin, J.H. Lee, B.K. Cho, S.H. Oh, J. Catal. 240 (2006) 47-57.

[10] J.A. Sullivan, J. Cunningham, M.A. Morris, K. Keneavey, Appl. Catal. B-Environ. 7 (1995) 137-151.

[11] H. Sjövall, E. Fridell, R. Blint, L. Olsson, Top. Catal. 42-43 (2007) 113-117.

[12] H.-Y. Chen, W.M.H. Sachtler, Catal. Today 42 (1998) 73-83.

[13] A.A. Battiston, J.H. Bitter, D.C. Koningsberger, J. Catal. 218 (2003) 163-177.

[14] S. Shwan, R. Nedyalkova, J. Jansson, J. Korsgren, L. Olsson, M. Skoglundh, Industrial & Engineering Chemistry Research 51 (2012) 12762−12772.

[15] S. Shwan, J. Jansson, J. Korsgren, L. Olsson, M. Skoglundh, Catal. Today 197 (2012) 24-37.

[16] S. Brandenberger, O. Kröcher, A. Tissler, R. Althoff, Applied Catalysis B: Environmental 95 (2010) 348-357.

[17] P. Marturano, L. Drozdová, A. Kogelbauer, R. Prins, J. Catal. 192 (2000) 236-247.

[18] A.A. Battiston, J.H. Bitter, F.M.F. de Groot, A.R. Overweg, O. Stephan, J.A. van Bokhoven, P.J. Kooyman, C. van der Spek, G. Vankó, D.C. Koningsberger, J. Catal. 213 (2003) 251-271.

[19] L. Kiwi-Minsker, D.A. Bulushev, A. Renken, J. Catal. 219 (2003) 273-285.

[20] J. Jia, K.S. Pillai, W.M.H. Sachtler, J. Catal. 221 (2004) 119-126.

[21] S. Shwan, E. Adams, J. Jansson, M. Skoglundh, Catal. Lett. 143 (2013) 43-48.

[22] S. Shwan, J. Jansson, L. Olsson, M. Skoglundh, Applied Catalysis B: Environmental 147 (2014) 111-123.

[23] S. Shwan, R. Nedyalkova, J. Jansson, J. Korsgren, L. Olsson, M. Skoglundh, Top. Catal. 56 (2013) 80-88.

[24] X. Feng, W.K. Hall, Catal. Lett. 41 (1996) 45-46.

[25] F. Heinrich, C. Schmidt, E. Löffler, M. Menzel, W. Grünert, J. Catal. 212 (2002) 157-172.

[26] Q. Zhu, R.M. van Teeffelen, R.A. van Santen, E.J.M. Hensen, J. Catal. 221 (2004) 575-583.

[27] R.Q. Long, R.T. Yang, Journal of the American Chemical Society 121 (1999) 5595-5596.

[28] M. Devadas, O. Kröcher, M. Elsener, A. Wokaun, G. Mitrikas, N. Söger, M. Pfeifer, Y. Demel, L. Mussmann, Catal. Today 119 (2007) 137-144.

[29] M. Iwasaki, K. Yamazaki, K. Banno, H. Shinjoh, J. Catal. 260 (2008) 205-216.

[30] R. Nedyalkova, S. Shwan, M. Skoglundh, L. Olsson, Applied Catalysis B: Environmental 138–139 (2013) 373-380.

[31] M.M.J. Treacy, J.B. Higgins, Collection of Simulated XRD Powder Patterns for Zeolites, 4 ed., ELSEVIER, 2001.

[32] B. Modhera, M. Chakraborty, P.A. Parikh, R.V. Jasra, Cryst. Res. Technol. 44 (2009) 379-385.

[33] C. He, Y. Wang, Y. Cheng, C.K. Lambert, R.T. Yang, Applied Catalysis A: General 368 (2009) 121-126.
[34] S. Brandenberger, O. Kröcher, A. Tissler, R. Althoff, Applied Catalysis A: General 373 (2010) 168-175.
[35] M.S. Kumar, M. Schwidder, W. Grünert, A. Brückner, J. Catal. 227 (2004) 384-397.
[36] S. Shwan, J. Jansson, L. Olsson, M. Skoglundh, In preparation (2014).
[37] G. Mul, M.W. Zandbergen, F. Kapteijn, J.A. Moulijn, J. Perez-Ramirez, Catal. Lett. 93 (2004) 113-120.
[38] G. Mul, J. Perez-Ramirez, F. Kapteijn, J.A. Moulijn, Catal. Lett. 80 (2002) 129-138.
[39] G. Spoto, A. Zecchina, G. Berlier, S. Bordiga, M.G. Clerici, L. Basini, J. Mol. Catal. A-Chem. 158 (2000) 107-114.
[40] D. Klukowski, P. Balle, B. Geiger, S. Wagloehner, S. Kureti, B. Kimmerle, A. Baiker, J.D. Grunwaldt, Applied Catalysis B: Environmental 93 (2009) 185-193.
[41] G.S. Qi, R.T. Yang, Appl. Catal. B-Environ. 60 (2005) 13-22.
[42] P.E. Petit, F. Farges, M. Wilke, V.A. Sole, J. Synchrot. Radiat. 8 (2001) 952-954.
[43] K. Krishna, M. Makkee, Catal. Today 114 (2006) 23-30.
[44] K. Segawa, Y. Chen, J.E. Kubsh, W.N. Delgass, J.A. Dumesic, W.K. Hall, J. Catal. 76 (1982) 112-132.
[45] G. Grubert, M.J. Hudson, R.W. Joyner, M. Stockenhuber, J. Catal. 196 (2000) 126-133.
[46] S.M. Park, G. Seo, Y.S. Yoo, H.S. Han, Korean J. Chem. Eng. 27 (2010) 1738-1743.
[47] M. Santhosh Kumar, M. Schwidder, W. Grünert, U. Bentrup, A. Brückner, J. Catal. 239 (2006) 173-186.

Table 1:

Peak assignment of DRIFT spectra during NO adsorption on H-BEA and Fe-BEA and UV-Vis assignment of the iron species

Peak position [cm^{-1}]	Assignment	Reference
1635	NO_2 on $Fe_x^{3+}O_y$	[29, 38, 46, 47]
1870	NO_x on oligomeric Fe_xO_y	[38, 44]
1880	NO_x on Fe^{3+} or Fe^{2+}	[38, 44-46]
2134	NO^+ on Fe^{3+} and Brønsted sites	[40-43]

Peak position [nm]	Assignment	Reference
234 (I) and 274 (II)	Monomeric iron	[34, 35]
328 (III) and 389 (IV)	Dimeric iron and Oligomeric, Fe_XO_Y	[34, 35]
466 (V)	Iron Particles, Fe_2O_3	[34, 35]

Table 2:

NO conversion during standard NH_3-SCR between 150 and 500^{0}C for 2 wt.% Fe-BEA from ref. [30]. Relative intensities of the deconvoluted UV-Vis spectra.

Temperature, °C	NO-conversion, %	
	Fresh sample	H_2-treated sample
150	2	2.1
200	16.5	24.5
250	54.5	71.5
300	87	90
400	95	92
500	98	94

UV-Vis Absorption region	Relative absorption, %	
	Fresh sample	H_2-treated sample
I	20.5	24.5
II	29.5	41
III	28.5	25
IV	9	3.5
V	12.5	6

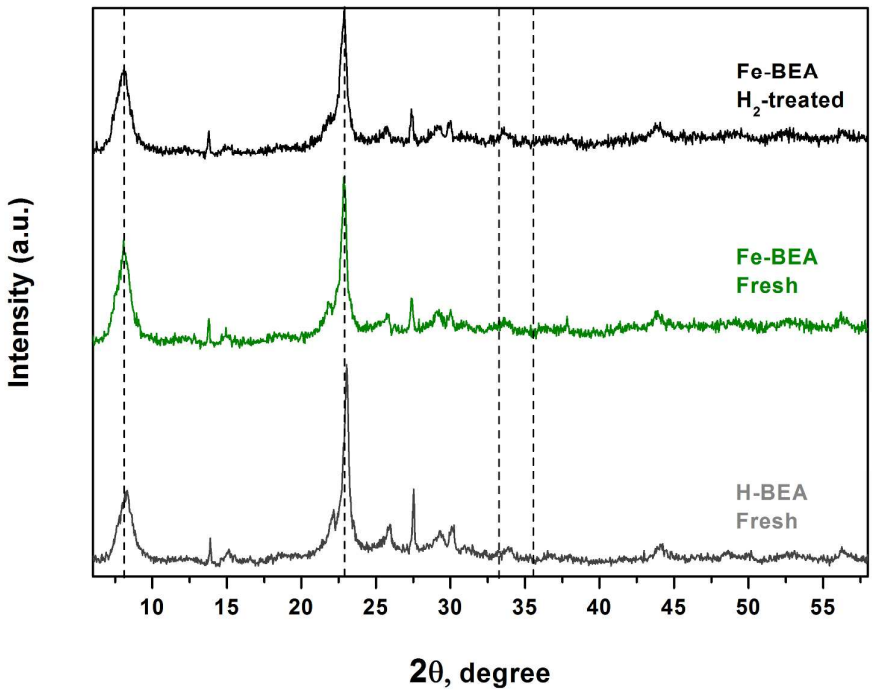

Figure 1: *X-ray diffraction spectra of fresh H-BEA and 2 wt. % Fe-BEA compared to H_2-treated 2 wt. % Fe-BEA catalysts. The position of the characteristic diffraction peaks for zeolite BEA and (iron oxide) Fe_2O_3 are marked at $2\theta = 7.74$ and 22.7^0, and at $2\theta = 33.2^0$ and 35.5^0, respectively.*

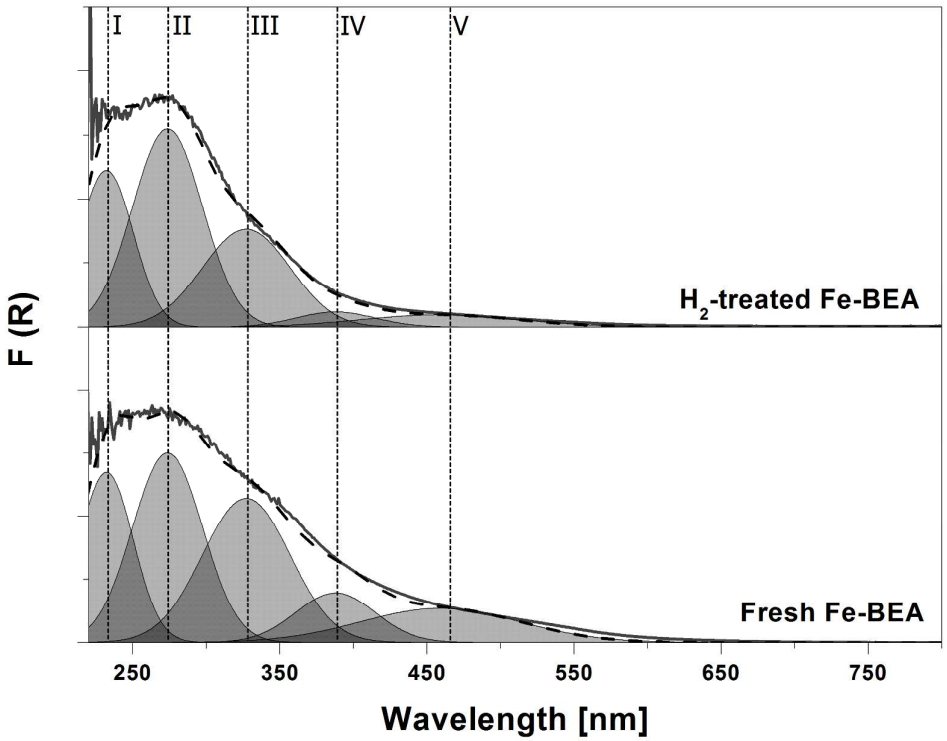

Figure 2: *UV-Vis spectra of iron from the fresh and H_2-treated 2 wt. % Fe-BEA powder sample after subtraction of the corresponding spectrum for H-BEA. The deconvoluted peaks **(I-II)** represent monomeric iron species (220-290 nm), (**III- IV**) dimeric and oligomeric iron species (300-400 nm), and (**V**) larger iron oxide particles (>400 nm).*

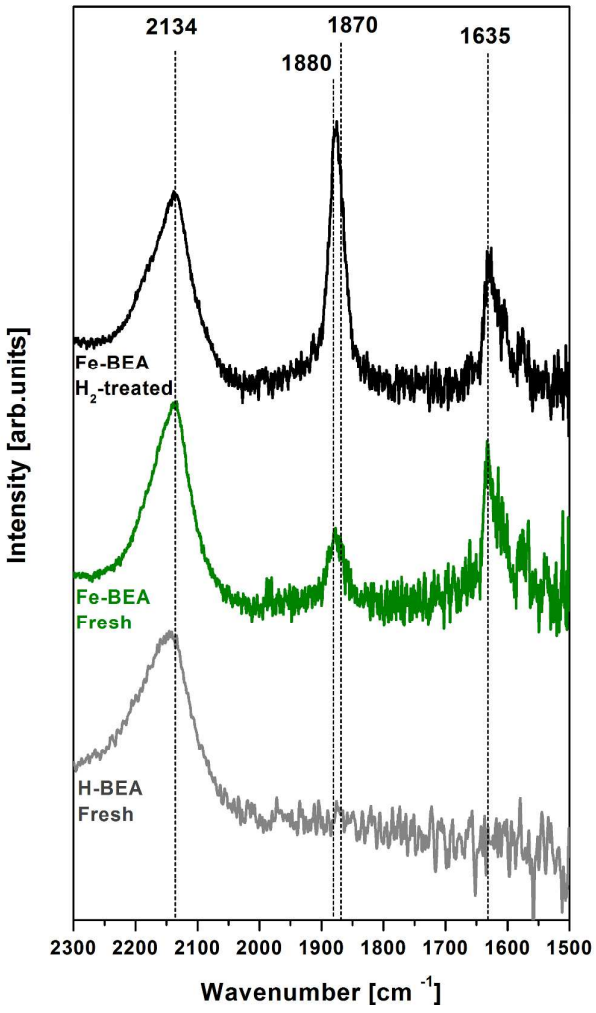

Figure 3: *DRIFT spectra of fresh H-BEA and Fe-BEA, and H_2-treated Fe-BEA samples, during exposure to 400 ppm NO and Ar (inert) at 150^0C for 30 min.*